Four-laser airborne infrared spectrometer for atmospheric trace gas measurements

J. Roths, T. Zenker, U. Parchatka, F. G. Wienhold, and G. W. Harris

We describe the four-laser airborne infrared (FLAIR) instrument, a tunable diode laser absorption spectrometer designed for simultaneous high-sensitivity *in situ* measurements of four atmospheric trace gases in the troposphere. The FLAIR spectrometer was employed during the large-scale airborne research campaign on tropospheric ozone (TROPOZ II) in 1991 and was used to measure CO, H_2O_2, HCHO, and NO_2 in the free troposphere where detection limits below 100 parts in 10^{12} by volume were achieved.

Key words: Tunable diode laser, absorption spectroscopy, airborne trace gas measurements.

1. Introduction

Progress in atmospheric chemistry research often is linked closely to the availability of new techniques for measuring trace gas concentrations in the atmosphere. Field studies of the chemical composition of the troposphere demand highly specific and sensitive analytical instrumentation. With *in situ* techniques, airborne operation is of great importance because the restriction on measuring primarily within the planetary boundary layer can be overcome, the vertical distribution over the full tropospheric height can be probed, and a large horizontal range can be covered within a short time period. Because of the aircraft velocity, the time response of an airborne sensor corresponds to the spatial resolution of the trace gas measurements. For example, ascent and descent from sea level to a flight altitude of 10 km takes approximately 40 min. Thus with a time resolution of 1 min, a vertical profile over the tropospheric height can be resolved by 40 individual measurements.

Tunable diode laser absorption spectroscopy (TDLAS) is a powerful technique that can provide high sensitivity, high selectivity, and fast time response trace gas measurements. Nearly all atmospheric gases of interest have strong absorption bands in the mid-infrared spectral region and are accessible with this technique. TDLAS has been employed frequently in atmospheric chemistry research in the past, and a large number of species have been measured both in laboratory and in field experiments.[1] Although a large number of TDLAS instruments have been built for trace gas detection, only a few airborne instruments have been constructed up to now, most of which are devoted to stratospheric research. Hastie and Miller[2] reported the first operation of a balloon-borne TDLAS system. Another airborne TDLAS system for stratospheric research was the balloon-borne laser *in situ* sensor, operated by Webster and co-workers at the Jet Propulsion Laboratory.[3] Two systems were designed to operate onboard NASA's high-altitude research aircraft ER-2. One system is the airborne tunable laser absorption spectrometer that was successfully employed during several Arctic and Antarctic measurement campaigns to determine N_2O as a stratospheric tracer.[4] The second ER-2-based instrument is the aircraft laser infrared absorption spectrometer that is also used mainly to study polar ozone chemistry by simultaneous measurements of HCl, NO_2, HNO_3, CH_4, and N_2O.[5] When the four-laser airborne infrared (FLAIR) instrument was designed, the only other operational instrument dedicated to tropospheric air chemistry research was the differential absorption CO monitor, which was initially designed for CO measurements onboard the NASA Electra aircraft and has been recently upgraded for simultaneous CO and CH_4 measurements[6,7] and for N_2O measure-

ments.[8] Schiff *et al.* reported a single-channel, high-sensitive airborne TDLAS instrument that was flown in 1986 onboard the NASA Electra aircraft as part of the global tropospheric experiment/chemical instrumentation and evaluation (GTE/CITE 2) program and was used to measure NO_2 and HNO_3.[9,10]

The abundance of several species of major importance as intermediates in atmospheric reaction cycles typically are below one part in 10^9 by volume. For example, the expected mixing ratios of formaldehyde, hydrogen peroxide, and nitrogen dioxide range between a few parts in 10^9 by volume (ppbv) and tens of parts in 10^{12} by volume (pptv). To have access to these species by TDLAS, minimum detectable absorbances of the order of 10^{-5}, combined with large absorption path lengths in the range of 100 m, have to be achieved under airborne conditions.

The FLAIR instrument described here is a TDLAS system that can be used to measure four trace gases simultaneously at high sensitivity, with a time resolution of the order of 1 min. It employs second derivative spectroscopy and is designed to have detection limits in the sub-ppbv range. The first deployment of the FLAIR spectrometer was in January 1991 during a large-scale airborne research campaign on tropospheric ozone (TROPOZ II).[11] In this research program, the FLAIR spectrometer was flown onboard a Caravelle F-116, a French research aircraft, operated by the Centre d'Essais en Vol, Brétigny. The scientific payload consisted of 14 instruments for in-flight trace gas monitoring developed by nine different French and German research institutes. During this campaign the FLAIR system was configured to measure CO, HCHO, H_2O_2, and NO_2. The goal of the research effort was to determine the large-scale distribution of a large number of trace gases. In this paper we use a data set of 5232 measurements, obtained during the TROPOZ II mission by the FLAIR instrument during 30 flights totaling 85 flight hours, to characterize the performance of the FLAIR system under field conditions.

2. Technique and Instrumentation

The mid-infrared spectral region (3–15 μm) contains the fundamental rovibronic transitions for many molecules of atmospheric interest and thus is well suited for spectroscopic trace gas determinations. Under atmospheric pressure one can determine the width of spectral lines by pressure broadening. For example, for NO_2 the pressure-broadening coefficient is $\gamma = (0.066 \pm 0.002)$ atm^{-1} cm^{-1} for the ν_3 absorption band.[12] With the well-known equation for Doppler broadening,[13] the relative influence of pressure and Doppler broadening on the width of the absorption line can be compared. At a pressure of $p = 0.02$ atm, Doppler and pressure broadening are of the same order of magnitude for the above-mentioned NO_2 molecule at room temperature. This gives the pressure range where the molecular absorption line shape is given by a Voigt profile and where single rovibronic absorption lines can be resolved, because for small molecules (2–5 atoms) the separations of the absorption lines typically are much larger than the Doppler width. At reduced pressure, for small molecules there is a high probability that absorption lines can be found that have no overlap with absorption lines from other species, resulting in an interference-free spectroscopic signal that is specific for the gas to be determined. This leads to the high selectivity of the TDLAS technique, which is a major advantage of this method. The line positions for the species measured during the TROPOZ II campaign are given in Table 1.

Table 1. Positions of Absorption Lines Used during the TROPOZ II Campaign with the FLAIR Spectrometer

Molecule	Wavelength/μm	Wave Number/cm^{-1}
H_2O_2	8.028	1245
NO_2	6.136	1629
HCHO	5.780	1730
CO	4.825	2073

For the diode lasers used, a single laser mode can be tuned continuously by current variation over ≥0.5 cm^{-1}, which is larger than the width of absorption lines under atmospheric conditions. The easy tunability of the laser wavelength is also used to enhance the system sensitivity by modulation techniques. Second harmonic detection has been used widely with TDLAS.[14–16] For the FLAIR instrument, a modulation frequency of 7.5 kHz is used, with signal detection at 15 kHz.

The FLAIR instrument consists of three main parts. The optical system contains the mid-infrared diode lasers, a folded absorption path length within a measurement cell, and the detector. The electronic subsystem provides the highly stable laser current, the temperature stabilization circuits for the diode lasers (which were operated at cryogenic temperatures), the signal lock-in amplification, and the data acquisition. The third part of the instrument is an automated calibration system.

A. Optical System

Special design requirements are needed for the instrument to operate onboard an airplane. The optical system has to be designed carefully to meet the stringent demands of vibration isolation, shock resistance, and weight minimization. Commercial optical components are not available to meet these requirements, so all optical components were designed specially for this application.

A schematic of the optical system is given in Fig. 1. All optical components are mounted on a 1.2 m × 0.6 m × 0.05 m honeycomb-structure optical table. The optical table is bolted onto the supporting structure with shock- and vibration-isolation mounts. The operating temperatures of lead-salt diode lasers typically are below 130 K. Therefore the tunable diode lasers are installed in four separate liquid-nitrogen Dewar devices, which provide the required cryogenic cooling. With a heating element and a temperature sensor diode, the laser temperature can be selected between 77 K (temperature of liquid ni-

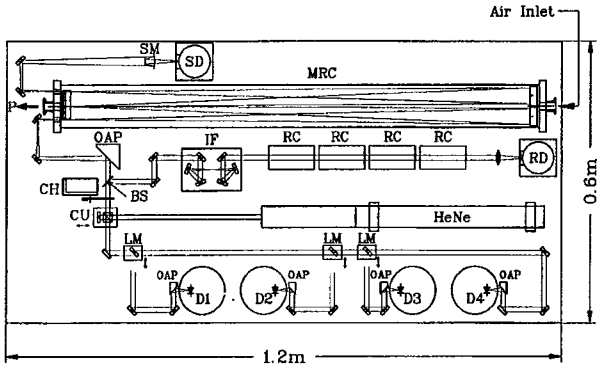

Fig. 1. Schematic of the optical setup. D1–D4, liquid-nitrogen Dewar with installed diode lasers; OAP, off-axis parabolic mirrors; LM, lifting mirrors; MRC, multiple reflection cell; SD, signal detector; BS, beam splitter; IF, intermediate focus; RC, reference cell; RD, reference detector; CH, chopper; HeNe, He–Ne laser; CU, coupling unit for He–Ne beam; SM, spherical mirror; P, pump.

trogen) and 130 K with a stability of better than 0.001 K. An operational hold time of approximately 4 h is achieved with a liquid-nitrogen content of 0.5 L at the highest accessible temperature. Four $f/2$ off-axis parabolic (OAP) mirrors collimate the divergently emitted laser beams. The diameter of the parallel laser beam is 15 mm, limited by the diameter of the OAP mirrors. One of the three magnetically driven vertically movable plane lifting mirrors (LM) and the fourth, fixed mirror selects one of the four laser beams. A CaF_2 window (beam splitter, BS) couples approximately 4% of the light intensity into a reference channel. As many as four reference cells (RC), containing high concentrations of the gases to be measured, are inserted in this channel. The strong absorption signals obtained at the reference detector (RD) are used to lock the emission frequency of the diode laser to the corresponding absorption lines. The intermediate focus (IF) point in the reference channel works as an interface where a miniaturized monochromator can be inserted. This monochromator is used to observe the mode characteristics of the diode lasers and gives an absolute wavelength readout. The main laser beam is directed to an OAP mirror, which provides the input focus for the multiple reflection cell, that has a volume of 6.4 L, a base length of 1 m, and provides an absorption path length of 126 m. An off-axis reflection on a spherical mirror (SM) in front of the liquid-nitrogen-cooled HgCdTe signal detector (SD) has two functions: first, it compensates for astigmatism that is generated by multiple off-axis reflections inside the cell, and, second, it focuses the laser beam on the active area of the signal detector. Important characteristics of the optical system are the mechanical stability and the immunity from unwanted étalon structures, which often originate in multiple reflection cells.

Étalon structures appear when uncontrolled, scattered, or reflected laser radiation, traversing a different optical path length than the principal beam, reaches the detector and interferes with the principal laser beam. If the laser wavelength is scanned across an absorption line, the interference will lead to a harmonic intensity modulation on the detector that overlays the intensity variation that is due to the molecular absorption to be measured. For high-sensitivity measurements, relative intensity variations of the order of $\Delta I/I_0 = 10^{-5}$ need to be measured. Therefore, étalon structures creating intensity variations of that order of magnitude degrade the absorption measurement. In this case the optical system acts as if a poor finesse étalon device is inserted in the optical path.

Unlike laser or detector noise, étalon structures have no statistical nature. Thus at increased measurement time the relative influence of laser and detector noise on the detection limit decreases, and unwanted étalon signals can be resolved with an increase in signal-to-noise ratio.

Several active schemes have been proposed to reduce étalon structures in diode laser absorption spectrometers. One method is to destroy the coherence of the laser light by the application of a mechanical vibration to one component of the optics.[17] In our approach no active étalon-fringe-removing scheme is applied. Our goal is to optimize the optical setup to avoid the occurrence of the étalon signals. Uncontrolled reflected light is reduced by the use of all-reflective optics. Special attention was given to the multiple reflection cell. Because of the complicated beam propagation in multiple reflection cells, these devices are often prone to the generation of unwanted étalon structures. The multiple reflection cell constructed for the FLAIR instrument is based on White's design.[18,19] Both the mechanical stability and the reduction of étalon structures are improved significantly by the addition of two corner cube mirrors to the three-mirror configuration. Figure 2 shows one end plate of the cell with the field mirror and the arrangement of the corner cube mirrors. This system is similar to that proposed by White,[19] but because of a different arrangement of the corner cube mirrors, the beam path and the mirror mounts are simplified, resulting in improved rigidity and smaller cell diameter. A further modification in our design is the location of the exit beam. In contrast to White's arrangement,[19] where the incoming and outgoing beams pass through the same window, the exit beam is fed through a separate window, resulting in a much simpler arrangement of the transfer optics and in an improved immunity against étalon structures because the spots on the mirror nearest to the exit beam are separated by a path difference that exceeds the laser coherence length.

B. Electronic System

Figure 3 shows a block diagram of the electronic system. Each diode laser is operated by a separate laser control unit (LCU) (Unisearch Association, Ontario, Canada), which can be used to control the temperature and the bias current of the diode laser. Remote control of the laser current is achieved by a voltage input to the LCU. This external voltage is

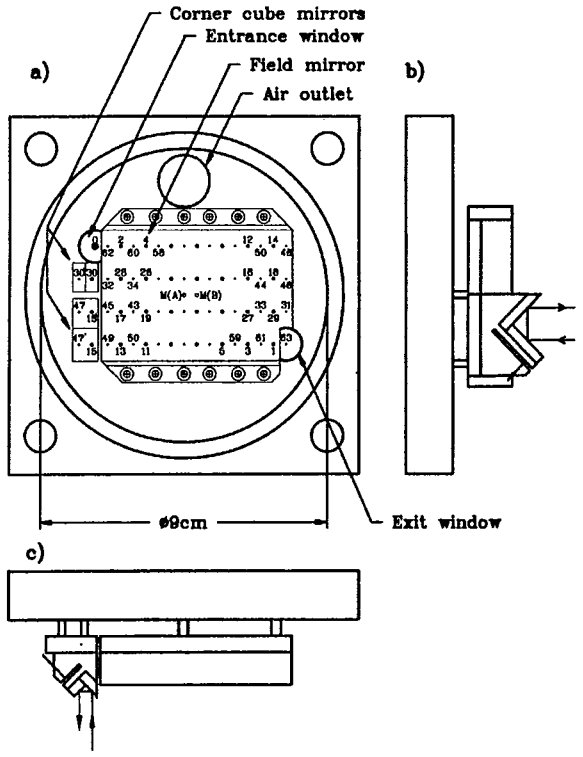

Fig. 2. End flange of the multiple reflection cell with field mirror and corner mirrors: a), front view, b), side view, c), top view. M(A) and M(B) are the centers of the opposed pair of spherical mirrors. The focus point of the incoming beam is indicated by 0, and the focus points on the field mirror are numbered according to their position in the beam path. The outgoing beam passes through a separate window behind focus point #63. The base length of the mirror system is 1 m, resulting in a total path length of 126 m.

transformed to a current that is added to the manually adjusted, constant laser bias current. We achieved the scanning of the diode laser output wavelength by applying a sawtooth signal (output port A1), which is generated by a microprocessor and a digital-to-analog converter (DAC), to the voltage input of the LCU. A 7.5-kHz triangle waveform generator supplies the modulation signal for the diode lasers. A combination with heating elements and temperature-sensing diodes installed on the laser mounts inside the liquid-nitrogen Dewars allows the laser control unit to stabilize the laser temperature to more than 0.001 K. The temperature set point of each diode laser can be changed by the microprocessor (output port A2). This is used for active locking of the laser wavelength to the absorption line. The absorption signal at the reference detector is amplified by a lock-in amplifier working in the $1f$ mode. The zero crossing of this $1f$ signal indicates the line center. This is detected by a discriminator, which produces a transistor–transistor logic signal. The microprocessor compares this line center signal with the center of the voltage ramp and calculates a correction for the temperature set point, which is in turn transferred to the LCU.

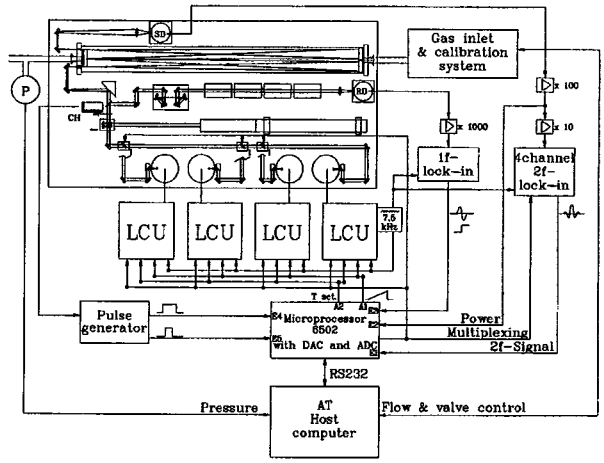

Fig. 3. Block diagram of the FLAIR spectrometer. LCU, laser control unit; SD, signal detector; RD, reference detector; P, pressure gauge; ADC, analog-to-digital converter; DAC, digital-to-analog converter; CH, chopper.

The amplification chain of the signal channel consists of two preamplification stages and a lock-in amplifier operating in the $2f$ mode. A multiplexing circuit selects four separate phase and gain settings for the lock-in amplifier when switching from one laser diode, i.e., molecule to be measured, to another. The amplified $2f$ absorption waveform is applied to the input channel E1 of the analog-to-digital converter (ADC). The signal behind the first preamplification stage in the signal channel is also applied to the input port E2 for monitoring the total laser power.

The duration of a measurement cycle is defined by the time period needed for one rotation of the chopper rotor, which is illustrated in Fig. 4. During one chopper rotation, which takes 70 ms, the laser beam is blocked for 5 ms. The resulting signal waveform at the microprocessor input port E2 is shown in Fig. 4. The amplitude of this signal is proportional to the laser power. After reading the laser power, the microprocessor starts the ramp current for sweeping the laser wavelength over the absorption line, while simultaneously the $2f$ absorption waveform is digitized into 128 channels and the zero crossing of the $1f$ signal, which marks the line center, is registered. Before the data are averaged we shift the observed $2f$ waveform by software until the zero-crossing signal matches the central ramp position. This compensates for small deviations in line position that may occur on time scales shorter than the active line-locking time constant.

Each laser is selected in turn every 18 s, which is of the order of the air exchange time in the cell. This ensures that the same air sample is probed by each channel, resulting in a quasi-simultaneous measurement. During the cycle time of 18 s, a total of 256 scans across the absorption lines are performed by all four channels. The number of scans for each channel can be selected by the operator, which determines

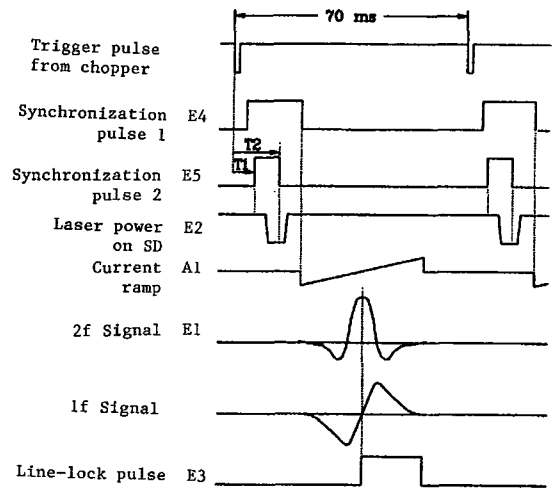

Fig. 4. Timing diagram. E1–E5 denote the input channels of the microprocessor control unit and A1 is an output channel (see Fig. 3). The repetition time of 70 ms is given by the rotation period of the chopper. The trigger signal generated by the chopper is shown on the upper trace. During one rotation, the chopper blocks the infrared beam for 5 ms, resulting in a decrease in optical power incident on the detector as shown in trace E2. The signals on E5, which are generated by the pulse generator, are used to trigger the microprocessor to read the total laser power. The trigger signal on E4 starts the ramp waveform generated by the DAC to sweep the laser across the absorption line. The detected $2f$ signal is shown on trace E1, whereas the zero crossing of the $1f$ signal is indicated by a transistor-transistor logic pulse on trace E3.

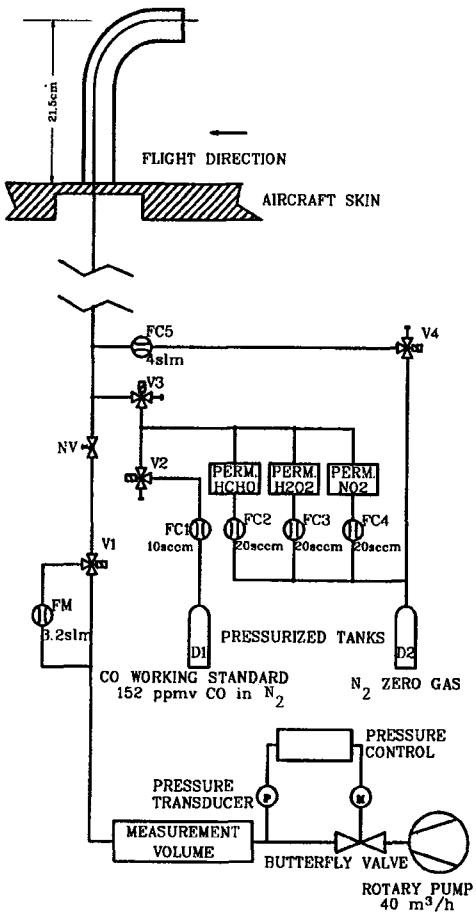

Fig. 5. Schematic of the gas flow and calibration system. FM, flow meter; FC, flow controler; V, valve, NV, needle valve; sccm, standard cubic centimeters per minute; slm, standard liter per minute.

the duty cycle for each channel. For the application described here, the carbon monoxide channel is active for 40 scans (corresponding to 2.6 s) and the other three channels for 72 scans (corresponding to 5 s) each. A preselected number of cycles is averaged before the spectra are transferred to a PC. Four cyles are averaged in the present application, which corresponds to 160 scans for CO and 288 scans for HCHO, H_2O_2, and NO_2, resulting in an overall time resolution of 72 s. The averaged spectra are displayed and stored on the PC. The PC also controls the gas flow and calibration system and monitors the pressure in the measurement volume.

C. Gas Flow and System Calibration

Figure 5 shows the computer-controlled gas flow and calibration system. To minimize surface loss effects, all lines at the incoming side of the measurement volume are made of Teflon material. Ambient air is sampled through a 3-mm-i.d. tube that is fed through a stainless-steel tube. To reduce contamination of the sample line by small particles or cloud droplets, the inlet faces away from the flight direction. The inlet point is located 215 mm from the aircraft surface, outside the aircraft boundary layer. A rotary pump with a pumping speed of 40 m^3/h drives the ambient air through the measurement cell. A needle valve (NV) creates a pressure drop while a servo-loop with a butterfly valve in front of the rotary pump and a capacitive pressure transducer stabilize the gas pressure inside the measurement volume at 40 hPa. The main gas flow, determined by the needle valve setting, is measured with a stainless-steel flow meter (FM), which is installed in a bypass. It is activated only during time periods when no absorption measurements are performed.

To determine the background spectrum, a surplus of pure N_2 gas, supplied by a pressurized tank (D2), is added to the inlet line. For calibration, known quantities of the gases to be measured are added to the N_2 gas stream. For CO, a working standard in a pressurized tank (D1) is used, and for HCHO, H_2O_2, and NO_2 permeation devices are used as gas sources. A carrier N_2 gas flow of 20 standard cubic centimeters per minute (sccm) is fed to the permeation devices by three separate flow controllers (FC2–FC4). For HCHO the permeation device consists of 1.5-cm, 3-mm-o.d. Teflon tubing filled with paraformaldehyde inside a glass cell that is temperature stabilized to 70 °C. During the first field application of the FLAIR spectrometer, we took advantage of a second independent HCHO measurement technique[20] that was also used on the TROPOZ II project. This technique is based on sampling formaldehyde on 2,4-dinitrophenyl

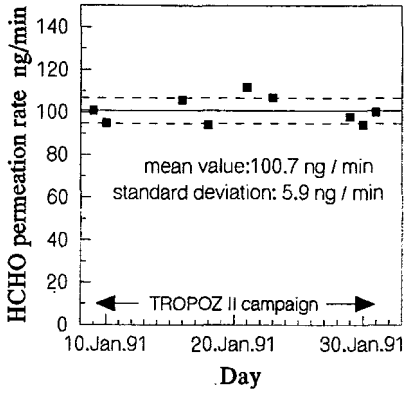

Fig. 6. Permeation rate of the HCHO source measured during the TROPOZ II campaign by the DNPH and HPLC technique.[20,21] The solid line indicates the mean value and the dashed lines give the 1σ interval.

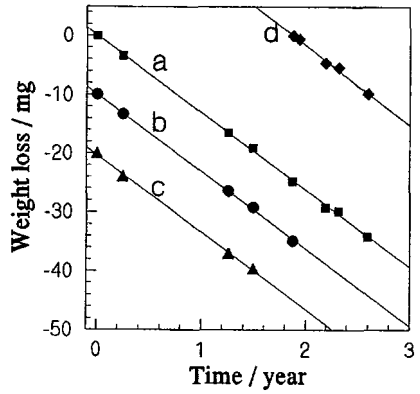

Fig. 7. Weight-loss determinations of the NO_2 permeation tube with four different high-precision balancies (a–d). An offset is added to each measurement series so as to have a clearer representation. The measurements from all balances agree well with each other. The permeation rate, determined by all measurement series, is 26.3 ± 0.18 ng/min.

hydrazine (DNPH) coated cartridges with subsequent high-performance liquid chromatography (HPLC) analysis. The output of the HCHO permeation cell was sampled on DNPH-coated cartridges. A total of nine samples were taken during the TROPOZ II campaign, a four-week period, and were analyzed after the campaign. The results of the DNPH and HPLC measurements are given in Fig. 6.[21] The samples gave a mean permeation rate of 100.7 ng/min with a standard deviation of 5.9 ng/min. No systematic deviation is observed whether the sample is taken before, during, or after a flight. This is in accordance with weight-loss measurements, performed before and after the measurement campaign, which yield a permeation rate of 98.3 (±3.2) ng/min. For calibration, the output of the permeation source is added to the main gas stream, which was typically 3.2 standard liter per minute (slm), resulting in a calibration mixing ratio of 23.5 ppbv within the measurement cell. This calibration method compensates for all first-order surface processes that may affect the throughput efficiency of the sampling line.

For NO_2 a permeation tube, supplied by VICI Metronics, was used and installed in a glass container at 40 °C. Precise determination of the weight loss with four different high-precision balances over a time period of 2 years before and 1 year after the TROPOZ II campaign gave a permeation rate of 26.3 ng/min with an uncertainty of 0.18 ng/min, as depicted in Fig. 7.

The permeation device for H_2O_2 consists of a polyethylene tubing coiled inside a glass cell containing a 30% H_2O_2 solution. The permeation rate was determined by titration with $KMnO_4$ as described by Zenker.[22] These measurements, shown in Fig. 8, revealed a decreasing permeation rate with time. An exponential function [$P = P_0 \exp(-at)$] was fitted to these data, giving a time-dependent permeation rate of $P_0 = 696$ ng/min for $t = 0$ and a time constant of $a = -0.033\ d^{-1}$. For the H_2O_2 measurements during the field campaign, the noon-time values of the exponential fit function were used daily.

For carbon monoxide, a commercially available working standard containing 152 parts in 10^6 by volume (ppmv) CO in N_2 was used. The accuracy of the mixture was 2%, as stated by the supplier. A mass flow controller (FC1) fed 5.4 sccm of the CO calibration gas to the main N_2 gas stream. In contrast to the other gases mentioned above, the nitrogen used as zero gas contained a small amount of carbon monoxide (see below). Therefore, the CO absorption signature of the carrier gas has to be subtracted from the signal created by the CO calibration gas plus carrier gas.

3. Data Revision and Evaluation Procedures

To assess the reliability of the measurements made during the first field application of the FLAIR spectrometer, a careful review of the data was performed. Several instrument parameters were recorded and stored on computer disk together with the observed absorption spectra. This allows reconstruction of the instrument status during all operation conditions. The monitored position of the butterfly valve gives

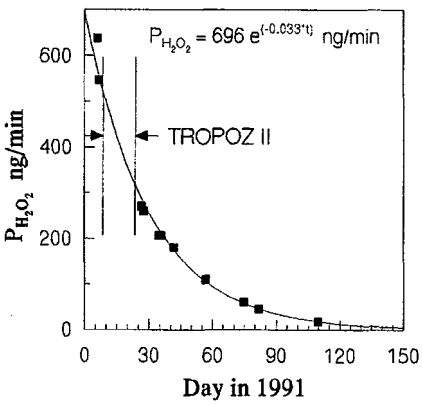

Fig. 8. Temporal behavior of the H_2O_2 permeation rate. The time interval of the TROPOZ II campaign is indicated. The solid curve represents the best fit of an exponential function to the measured values.

information about the correct control of the pressure-stabilizing loop. Data obtained during periods of unstable pressure were rejected. Another housekeeping parameter is the laser power incident on the signal detector. Decreasing laser power indicates changes in the optical alignment. During the TROPOZ II campaign, laser power variations were in the range of a few percent, indicating no major misalignments caused by mechanical instabilities of the optical setup. All absorption signals are normalized to a common power value. The next step of the revision procedure was used to examine the reliability of the calibration signals. Instrument calibration was performed before, during, and after a flight. The calibration method, as described above, assumes that the main gas flow is constant during the calibration procedure. During ascending or descending flight segments, the pressure inside the measurement cell is held constant by the pressure control loop while the outside pressure and the main gas flow change. As a result, the calibration mixing ratio provided by the dilution-type calibration system is unstable. Thus valid in-flight calibrations can be performed only during constant altitude flight segments. Automatic calibrations inadvertently made during ascents or descents have to be rejected. It was found that approximately 8% of all calibrations performed during the TROPOZ II campaign were not taken during constant altitude intervals. For all but one flight leg of the campaign, at least two valid in-flight calibrations remained so that only a small amount of data were lost due to missing calibration.

Measured absorption spectra obtained during the TROPOZ II campaign on different flight legs are shown in Figs. 9(a)–9(d). Figure 9(a) gives an example of an absorption signal of carbon monoxide. The solid curve is a two-parameter fit of the calibration signal S_{cal} to the ambient air absorption signal S_{amb}, where the fit parameter p_1, together with the mixing ratio of the calibration signal $\langle CO \rangle_{cal}$, gives the CO mixing ratio of the ambient air $\langle CO \rangle_{amb} = \langle CO \rangle_{cal} p_1$.

Carbon monoxide, which has mixing ratios greater than 50 ppbv in the free troposphere, always shows high signal-to-noise ratios, so the quality of these measurements are not determined by the detection limit of the spectrometer; the stability of the calibration factor is more important. This issue is addressed in Fig. 10, which shows the relative magnitude of all CO zero gas signals obtained during Flight 7 obtained while the FLAIR instrument measured the background spectra in the other three channels. As mentioned above, the N_2 zero gas has a constant abundance of carbon monoxide, therefore it can be regarded as a secondary calibration standard for the CO channel. The relative amplitudes of the absorption signals represent the variation of the CO calibration factor during the flight. For Flight 7 the total variation of the calibration factor is approximately 20%, which was the worst case for all the flights. The variation was typically of the order of 10%. Laboratory investigations revealed that possible sources for this variation are thermal drift of the gain or phase of the lock-in amplifier or a drift of the temperature–current working point of the diode under line-locking conditions. The influence of these effects on the measured CO mixing ratios is reduced

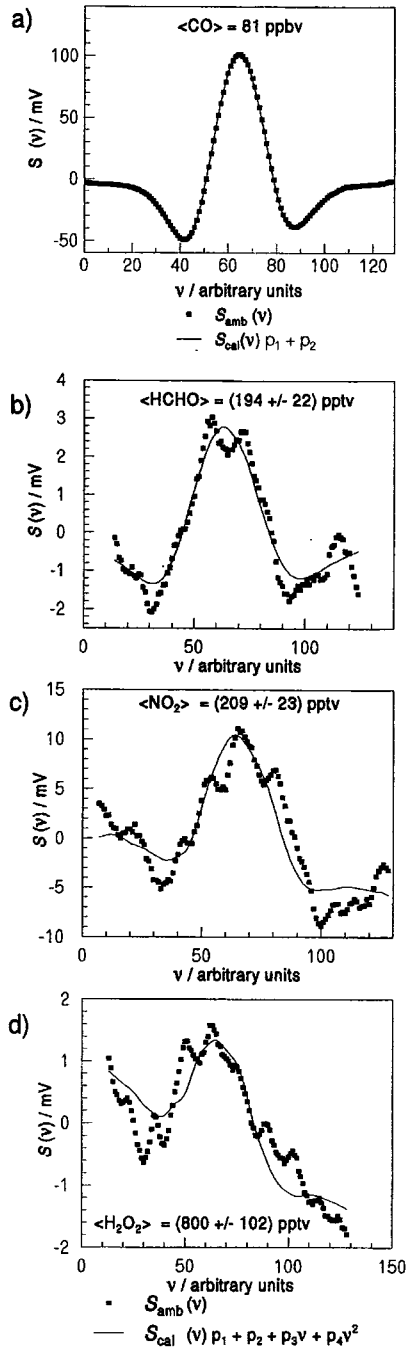

Fig. 9. Typical 2*f* absorption signals (filled boxes) observed during the TROPOZ II campaign for a) carbon monoxide (21.2 °N, 62.4 °W, 8.21-km altitude); b) formaldehyde (31.4 °N, 64.2 °W, 5.44-km altitude); c) nitrogen dioxide (29.0 °N, 15.1 °W, 6.19-km altitude); and d) hydrogen peroxide (20.8 °S, 41.9 °W, 8.73-km altitude). The solid curves are the fits of the calibration signals (plus a second-order polynomial for background approximation) to the data points.

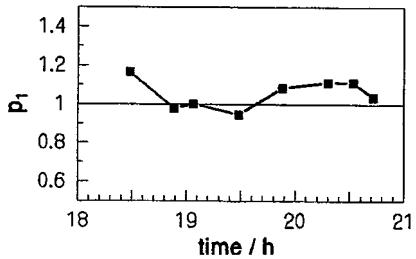

Fig. 10. Variation of the instrument calibration factor during one flight. The relative amplitudes of the CO absorption of a secondary calibration standard (N_2 zero gas) is shown as a function of time. The drift in the instrument calibration factor can be addressed by the application of a time-dependent calibration factor, which is given by the polygon line.

by the application of a time-dependent calibration coefficient to the measured CO absorption features. The time dependence is approximated by linear interpolation between the measured absorption signals from the zero gas, as indicated by the polygon in Fig. 10. It is estimated that the remaining relative uncertainty in the calibration factor, which has to be applied for each individual ambient air CO measurement, is of the order of 5%. To this the statistical uncertainty of the fit parameter, which was typically of the order of 1%, has to be added, resulting in a precision of 5.2%. For an estimation of the accuracy, the uncertainties of the gas flow meters and the calibration gas have to be added, resulting in an overall accuracy of the CO measurements of 6.3%.

Because of their low concentrations in the free troposphere, the absorption signals of HCHO, NO_2, and H_2O_2 have a much poorer signal-to-noise ratio than the carbon monoxide absorption signals. This is apparent in Figs. 9(b)–9(d), where typical in-flight absorption features of HCHO, NO_2, and H_2O_2 are shown. The $2f$ absorption signals are distorted by a background structure. Both variations of the laser output power with wavelength and étalon structures generated by scattered laser power inside the optical system contribute to the background structure. The power variation with wavelength is a fundamental characteristic of an individual diode laser at a given temperature and current working point. The laser diodes and the temperature and current working points are selected carefully and optimized to minimize power variation within the wavelength scanning range at a strong, interference-free absorption of the target species. Although étalon structures are suppressed by the special design of the optical system, as described above, small misalignments can lead to residual étalon structures. The filled boxes in Figs. 9(b)–9(d) represent the measured ambient air signals $S_{amb}(\nu)$, and the solid curves are a fit function $f(\nu)$, which is the sum of the calibration signal $S_{cal}(\nu)$ and a second-order polynomial:

$$f(\nu) = S_{cal}(\nu)p_1 + p_2 + p_3\nu + p_4\nu^2. \quad (1)$$

The polynomial describes a curved, sloping background that can vary from spectrum to spectrum.

Table 2. Detection Limits of the FLAIR Spectrometer[a]

Species	Figure	$\langle x\rangle_{amb}$ (ppbv)	SNR	$\langle x\rangle_{min} = \frac{\langle x\rangle_{amb}}{SNR}$ (ppbv)
HCHO	9(b)	0.194	9.0	0.022
NO_2	9(c)	0.209	7.7	0.027
H_2O_2	9(d)	0.800	4.5	0.177

[a]Based on the examples of Figs. 9(b)–9(d).

Only the parameter p_1 is used, together with the mixing ratio of the species x during calibration $\langle x\rangle_{cal}$, to calculate the ambient air mixing ratio $\langle x\rangle_{amb} = \langle x\rangle_{cal}p_1$. The detection limit of the species x is defined as the mixing ratio that can be observed with a signal-to-noise (SNR) ratio of 1:

$$\langle x\rangle_{min} = \langle x\rangle_{SNR=1}. \quad (2)$$

Although this definition is well accepted, there is less consensus among tunable diode laser practitioners about a standard procedure as to how the detection limit should be derived from measurements. One approach for estimating the detection limits is applied to the examples of Figs. 9(b)–9(d). The standard deviation of the difference of the measured values and the corresponding values of the fit function

$$\sigma = \frac{1}{n-1}\left(\sum_{i=1}^{n}\{S_{amb}(\upsilon_i) - [S_{cal}(\upsilon_i)p_1 + p_2 + p_3\upsilon_i + p_4\upsilon_i^2]\}^2\right)^{1/2}, \quad (3)$$

are taken as a measure of the noise. The signal-to-noise ratio can be quantified by the ratio of the amplitude of the fit function $S^0_{cal}\,p_1$ and σ (SNR = $S^0_{cal}\,p_1/\sigma$). With these definitions, the estimates for the detection limits, based on the observed absorption signals from Figs. 9(b)–9(d), can be calculated and are given in Table 2. This approach to estimating the detection limits can be applied only to measurements that are close to the detection limit. Otherwise the estimation would be based on a division of two large quantities, resulting in a large uncertainty of the estimate. Therefore the examples of Figs. 9(b)–9(d) are selected to show mixing ratios not more than a factor of 10 larger than the detection limit. We note that the above-mentioned estimates for the detection limit are based on individual absorption measurements, and small misalignments can degrade the detection limit. Therefore the above-mentioned figures demonstrate the detection limits that can be achieved under field operation conditions with the FLAIR spectrometer. A continuous monitoring of the detection limits during instrument operation is not possible due to the above-mentioned limitation of the procedure. The precision of the measured HCHO, NO_2, and H_2O_2 depends on how close the mixing ratios are to the detection limit. The accuracy is determined by the uncertainty of the permeation rate and the gas flow during calibration and can

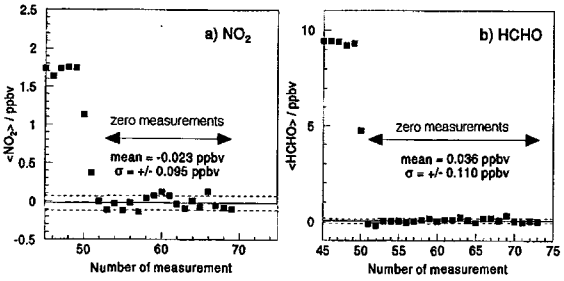

Fig. 11. Laboratory investigations that show the performance of the FLAIR spectrometer in the vicinity of the detection limits a) for the NO_2 channel and b) for the HCHO channel. During the first five measurements, calibration gas was introduced into the measurement cell before it was switched off, and pure nitrogen gas remained in the cell (zero measurements). The data-processing software handled all measurements as ambient air measurements. The variation in the zero measurements can be used to characterize the performance of the instrument when it is operating close to the detection limits.

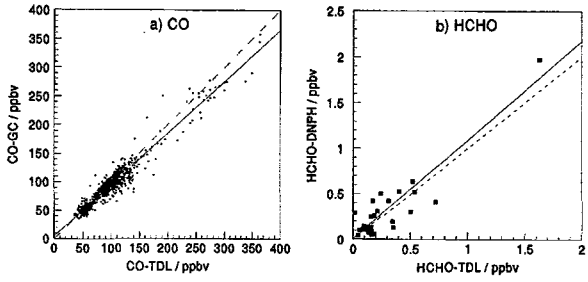

Fig. 12. Airborne intercomparison of carbon monoxide and formaldehyde measurements made with the FLAIR spectrometer during the TROPOZ II campaign. Carbon monoxide is compared with gas chromatography measurements (GC) and formaldehyde is compared with a DNPH technique. The solid lines are least-squares fits ($y = a + bx$) to the data points, and the dashed lines give the $y = x$ identity for reference. The statistics describing the regression lines are given in Table 3. TDL, tunable diode laser.

be estimated to be 7.5% for the HCHO, NO_2, and H_2O_2 channels.

Further laboratory investigations were performed to characterize the FLAIR spectrometer and are shown in Figs. 11(a) and 11(b). They depict simultaneous measurements made with the NO_2 and HCHO channels of the FLAIR spectrometer. The acquisition time was 1 min (30 s for each channel). The first five data points in each data set were obtained by the introduction of calibration gas plus pure nitrogen into the measurement volume. At data point #49 the calibration gas was shut off and only pure nitrogen gas remained in the measurement cell. The data were still handled as normal ambient air measurements by the data evaluation procedure, with the calibration signals and the polynomial fitted to all measured signals. The first data points represent the mixing ratio during instrument calibration, whereas the other data, the so-called zero measurements, scatter at around zero. The average value of the zero measurements is -0.023 ± 0.095 (1σ) ppbv for NO_2 and $+0.036 \pm 0.110$ (1σ) ppbv for HCHO. The mean values of the zero measurements are within the 1σ interval around zero and are comparable to the detection limits stated above. These investigations demonstrate that mixing ratios as low as 100 parts in 10^{12} by volume of HCHO and NO_2 can be measured with the FLAIR spectrometer with a time resolution of 1 min.

During the TROPOZ II campaign carbon monoxide and formaldehyde were also measured onboard the research aircraft by other techniques, which provided an opportunity for comparison. Carbon monoxide was measured by Marenco[23] with a gas chromatography (GC) technique, and formaldehyde was measured by Arlander *et al.*[20] with DNPH-coated cartridges and subsequent HPLC analysis. The integration time of the FLAIR spectrometer was approximately 1 min, the time resolution of the CO–GC measurements was 0.5 min and of the HCHO–DNPH measurements 20 min. Data with a shorter integration time were averaged to coincide with the sampling time of the other measurement technique. Figure 12 shows the scattergrams for both gases. The solid lines in Fig. 12(a) and 12(b) are least-squares fits ($y = a + bx$) to the data points and the dashed lines give the $y = x$ identity for reference. The statistics describing the regression lines are given in Table 3.

For carbon monoxide the high correlation coefficient of $r = 0.965$, together with the large number of samples, describes the good correlation between both techniques. The intercept ($a = 5.1 \pm 10.4$ ppbv) is within its standard deviation compatible with the origin. Within the limits of this statistical analysis, a constant bias between the respective CO data sets can be ruled out. The slope of $b = 0.900 \pm 0.008$ shows a deviation from the ideal value of $b = 1$, which is outside of its statistical uncertainty. This linear bias can be associated with a 10% deviation between the CO working standards used in each experiment. This is within the 2σ interval of the combined uncertainty stated by the suppliers of each CO working standard.

The formaldehyde intercomparison also shows good correlation. The number of data points is much more limited due to the fact that in the free troposphere the formaldehyde mixing ratio was often below the detection limit of the FLAIR spectrometer. We note that under strongly polluted conditions, the DNPH technique showed larger values than the TDLAS technique by more than a factor of 2. A possible reason for this discrepancy is an interference in

Table 3. Parameters of the Regression Lines Shown in Figs. 12(a) and 12(b)

Parameter	Carbon Monoxide	Formaldehyde
a (intercept)	5.1 ppbv	0.008 ppbv
σ_a	±10.4 ppbv	±0.058 ppbv
b (slope)	0.900	1.082
σ_b	±0.008	±0.092
r (correlation coefficient)	0.965	0.914
N (number of data points)	1038	29

the DNPH method to higher aldehydes and other hydrocarbons.[20] Therefore data obtained under highly polluted conditions are omitted in the HCHO intercomparisons shown above, and only values obtained in the free troposphere are included.

4. Conclusion

The FLAIR spectrometer is a powerful new tool for high-sensitivity airborne measurement of tropospheric trace gases. With the replacement of the diode lasers it can easily be reconfigured to measure other trace gases such as CH_4, N_2O, CO_2, and HNO_3. The data set obtained during the TROPOZ II campaign by the FLAIR spectrometer is reported elsewhere.[24,25] In 1992 the FLAIR spectrometer was employed successfully onboard a DC-3 aircraft as part of the Southern Africa five atmospheric research initiative project to study the influence of biomass burning in the southern part of Africa.[26] In 1993 and 1994 the FLAIR system was used as a ground-based system for several field measurement campaigns (field studies of the tropospheric degradation mechanisms of biogenic volatile organic compounds and oxidizing capacity of the tropospheric atmosphere) in Europe.[27]

References

1. H. I. Schiff, G. I. Mackay, and J. Bechara, "The use of tunable diode laser absorption spectroscopy for atmospheric measurements," in *Air Monitoring by Spectroscopic Techniques*, M. W. Sigrist, ed. (Wiley, New York, 1994).
2. D. R. Hastie and M. D. Miller, "Balloon-borne tunable diode laser absorption spectrometer for multispecies trace gas measurements in the stratosphere," Appl. Opt. **24,** 3694–3701 (1985).
3. C. R. Webster and R. D. May, "Simultaneous in-situ measurements and diurnal variations of NO, NO_2, O_3, $j(NO_2)$, CH_4, H_2O, and CO_2 in the 40- to 26-km region using an open path tunable diode laser spectrometer," J. Geophys. Res. D **10,** 11931–11950 (1987).
4. J. Podolske and M. Loewenstein, "Airborne tunable diode laser spectrometer for trace-gas measurement in the lower stratosphere," Appl. Opt. **32,** 5324–5333 (1993).
5. C. R. Webster, R. D. May, C. A. Trimble, R. G. Chave, and J. Kendall, "Aircraft (ER-2) laser infrared absorption spectrometer (ALIAS) for in-situ stratospheric measurements of HCl, N_2O, CH_4, NO_2, and HNO_3," Appl. Opt. **33,** 454–472 (1994).
6. G. W. Sachse, G. F. Hill, L. O. Wade, and M. G. Perry, "Fast-response, high-precision carbon monoxide sensor, using a tunable diode laser absorption technique," J. Geophys. Res. D **92,** 2071–2081 (1987).
7. R. C. Harriss, G. W. Sachse, G. F. Hill, L. Wade, K. B. Bartlett, J. E. Collins, L. P. Steele, and P. C. Novelli, "Carbon monoxide and methane in the North American Arctic and Subarctic troposphere: July–August 1988," J. Geophys. Res. D **97,** 16589–16599 (1992).
8. G. W. Sachse, Atmospheric Science Division, NASA Langley Research Center, Hampton, Va. (personal communication, 1996).
9. H. I. Schiff, D. R. Karecki, G. W. Harris, D. R. Hastie, and G. I. Mackay, "A tunable diode laser system for aircraft measurements of trace gases," J. Geophys. Res. D **95,** 10147–10153 (1990).
10. M. A. Carroll, D. R. Hastie, B. A. Ridley, M. O. Rodgers, A. L. Torres, D. D. Davis, J. D. Bradshaw, S. T. Standholm, H. I. Schiff, D. R. Karecki, G. W. Harris, G. I. Mackay, G. L. Gregory, E. P. Condon, M. Trainer, G. Hubler, D. D. Montzka, S. Madronich, D. L. Albritton, H. B. Singh, S. M. Beck, M. C. Shipham, and A. S. Bachmeier, "Aircraft measurements of NO_x over the Eastern Pacific and continental United States and implications for ozone production," J. Geophys. Res. D **95,** 10205–10233 (1990).
11. A. Marenco, I. Jonquières, H. Gouget, and P. Nédélec, "Experimental determinations of meridional distribution and long term evolution of tropospheric ozone—consequences on radiative forcing," in *Atmospheric Ozone as a Climate Gas*, W.-C. Wang and I. S. A. Isaksen, eds., Vol. I32 of NATO ASI Series (Springer-Verlag, Berlin, 1995), pp. 305–319.
12. V. Malathy Devi, B. Fridovich, G. D. Jones, D. G. S. Snyder, P. D. Palash, J.-M. Flaud, C. Camy-Peyret, and K. Narahari Rao, "Tunable diode laser spectroscopy of NO_2 at 6.2 μm," J. Mol. Spectrosc. **93,** 179–195 (1982).
13. W. Demtröder, *Laser Spectroscopy* (Springer-Verlag, Berlin, 1982).
14. J. Reid, B. K. Garside, J. Shewchun, M. El-Sherbiny, and E. A. Ballik, "High sensitivity point monitoring of atmospheric gases employing tunable diode lasers," Appl. Opt. **17,** 1806–1810 (1978).
15. J. Reid, M. El-Sherbiny, B. K. Garside, and E. A. Ballik, "Sensitivity limits of a tunable diode laser spectrometer with application to the detection of NO_2 at the 100 pptv level," Appl. Opt. **19,** 3349–3353 (1980).
16. J. Reid and D. Labrie, "Second-harmonic detection with tunable diode lasers: comparison of experiment and theory," Appl. Phys. B **26,** 203–210 (1981).
17. C. R. Webster, "Brewster plate spoiler: a novel method for reducing the amplitude of interference fringes that limit tunable laser absorption sensitivities," J. Opt. Soc. Am. B **2,** 1464–1470 (1985).
18. J. U. White, "Long optical paths of large aperture," J. Opt. Soc. Am. **32,** 285–291 (1942).
19. J. U. White, "Very long optical paths in air," J. Opt. Soc. Am. **66,** 411–416 (1976).
20. B. Arlander, D. Brüning, U. Schmidt, and D. H. Ehhalt, "The tropospheric distribution of formaldehyde during TROPOZ II," J. Atmos. Chem. **22,** 257–268 (1995).
21. B. Arlander, IVL Institutet för Vattenoch Luftvardsforskning, Swedish Environmental Research Institute, S-40258 Göteborg, Sweden (personal communication, 1992).
22. T. Zenker, "Absorptionsspektroskopische Messungen troposphärischer Spurengase in der bodennahen Grenzschicht über dem Atlantik," Ph.D. dissertation (University Mainz, Mainz, Germany, 1990), Chap. 3.4.3, pp. 96–101.
23. A. Marenco, Laboratoire d'Aérologie, CNRS, 31400 Toulouse, France (personal communication, 1992).
24. J. Roths, "Entwicklung eines flugtauglichen, laserspektroskopischen Spurengassensors und dessen Einsatz bei der TROPOZ-II-Flugmesskampagne," Ph.D. dissertation (University Mainz, Mainz, Germany, 1992).
25. J. Roths and G. W. Harris, "The tropospheric distribution of carbon monoxide as observed during the TROPOZ II experiment," J. Atmos. Chem. **24,** 157–188 (1996).
26. G. W. Harris, T. Zenker, and F. Wienhold, "Airborne observation of strong biogenic NO_x emissions from the Namibian Savanna during SAFARI 92," J. Geophys. Res. to be published.
27. H. Fischer, R. Zitzelsberger, T. Zenker, J. Roths, D. Trapp, H. Harder, A. Volz-Thomas, and G. W. Harris, "Development and application of multi-laser TDLAS instruments for groundbased, shipboard, and airborne measurements in the troposphere: field intercomparisons with other methods for CO, HCHO, and NO_2," in *Proceedings of the Eurotrac '96 Symposium*, P. M. Borrell, P. Borell, T. Cvitas, K. Kelly, and W. Seiler, eds. (Computational Mechanics, Southampton, U.K., 1996).